JCTC Journal of Chemical Theory and Computation

pubs.acs.org/JCTC Article

# Measuring Density-Driven Errors Using Kohn–Sham Inversion

Seungsoo Nam, Suhwan Song, Eunji Sim,* and Kieron Burke

Cite This: J. Chem. Theory Comput. 2020, 16, 5014–5023 Read Online

ACCESS | Metrics & More | Article Recommendations | Supporting Information

**ABSTRACT:** Kohn–Sham (KS) inversion, that is, the finding of the exact KS potential for a given density, is difficult in localized basis sets. We study the precision and reliability of several inversion schemes, finding estimates of density-driven errors at a useful level of accuracy. In typical cases of substantial density-driven errors, Hartree–Fock density functional theory (HF-DFT) is almost as accurate as DFT evaluated on CCSD(T) densities. A simple approximation in practical HF-DFT also makes errors much smaller than the density-driven errors being calculated. Two paradigm examples, stretched NaCl and the HO·Cl$^-$ radical, illustrate just how accurate HF-DFT is.

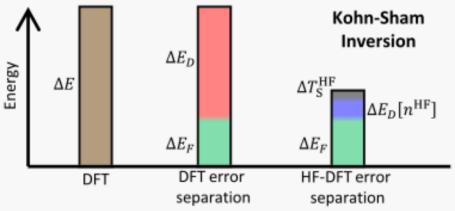




## 1. INTRODUCTION

Kohn–Sham (KS) density functional theory (DFT)[1] is an extremely popular approach to electronic structure problems, but the quality of the results depends on the quality of the exchange–correlation (XC) approximation used. Because the KS equations are solved self-consistently, there are errors in both the self-consistent (SC) energy and the SC density.[2] In most KS calculations, the density errors contribute little to the overall energy error. However, in various generic situations, semilocal approximations to XC make unusually large density errors (called density-driven errors) and the density error contributes significantly to the resulting energy error. In modern DFT parlance, these are attributed to delocalization errors[3] of the density.[4−6]

The theory behind density-corrected (DC) DFT explains the origin of such errors, when they are likely to be significant, and how they can usually be reduced by using a more accurate density.[2,7,8] The exact density-driven error is defined as the difference in energy when the approximate functional is evaluated on its SC and exact densities. If the exact density was needed to perform a DC-DFT calculation, the procedure would be impractical as finding a highly accurate density is more costly than the DFT calculation itself. However, in practice, for many semilocal approximations applied to molecular properties, it has been found that most density-driven errors can be greatly reduced by use of the Hartree–Fock (HF) density instead of the exact density. As the HF density is of comparable cost to DFT, this leads to a very practical approach (HF-DFT), which can be implemented very rapidly and costs no more than a typical DFT calculation.[9] HF-DFT has been used to reduce density-driven errors for electron affinities,[10] potential energy curves,[11,12] spin gaps for coordination compounds,[13] and noncovalent interactions.[14]

Given these successes of HF-DFT, we now ask: can its underlying assumptions be tested? The most important assumption is that, when density-driven errors are significant, in molecules, the HF density yields more accurate energies than the SC density. A lesser assumption is that, in practical HF-DFT calculations, the differences between HF and KS kinetic energies are ignored. The answer is yes, by employing the well-established technique of KS inversion to highly accurate densities, in order to extract exact density-driven errors and compare with the HF-DFT procedure. KS inversion is the process of finding an accurate KS potential (and associated objects, such as KS kinetic energy, HOMO, *etc.*) from a given density. From very early on,[15] method-developers in DFT have sought such exact information.[16−21] However, most such inversions have been focused on specific quantities such as eigenvalues, which can be very sensitive to the details of the density.

Here, we apply standard KS inversion procedures with the sole focus of testing the assumptions underlying HF-DFT. We use inversions to calculate density-driven errors for typical systems in which HF-DFT has proven successful. With two standard methods, we explore both the dependence on the basis set and the guiding density functional used (defined later). However, there are well-documented difficulties[22−25] when such inversions are performed in finite localized basis sets. We find that methods to overcome such difficulties, while imprecise, yield sufficient accuracy to answer the most basic questions about the density-driven error. These methods, applied to HF and high-level *ab initio* densities in standard basis sets, produce sufficiently accurate density-driven error estimates to usefully address such questions, that is, their remaining errors are small relative to common density-driven

Received: April 20, 2020
Published: July 15, 2020





https://dx.doi.org/10.1021/acs.jctc.0c00391
J. Chem. Theory Comput. 2020, 16, 5014−5023

errors. We also find that the approximation used in practical HF-DFT calculations, namely, using the HF kinetic energy instead of the KS kinetic energy, typically leads to changes of 1−2 kcal/mol, which is below a standard threshold for declaring a density-driven error.[26]

The paper is organized as follows. In Section 2, we present backgrounds about wavefunctions and KS-DFT, KS inversion, and DC-DFT. Section 3 shows inversion results and gives some discussions about the uncertainty of the inversion, together with testing DC-DFT. Finally, we deduce our conclusion from the discussions.

## 2. BACKGROUND

**2.1. Wavefunctions and KS-DFT.** Start from the variational principle for the exact ground-state energy

$$E_v = \min_{\Psi} \langle \Psi | \hat{H} | \Psi \rangle \tag{1}$$

where $\hat{H}$ is the $N$-electron Hamiltonian with one-body potential $v(\mathbf{r})$, and the search is over all antisymmetric, normalized many-body wavefunctions $\Psi$. An HF calculation uses only a single Slater determinant, denoted $\Phi$ (assuming for now no symmetry breaking)

$$E_v^{\mathrm{HF}} = \min_{\Phi} \langle \Phi | \hat{H} | \Phi \rangle \tag{2}$$

where $\Phi_v^{\mathrm{HF}}$ denotes the minimizer. The traditional definition of the correlation energy is then

$$E_{\mathrm{C},v}^{\mathrm{trad}} = E_v - E_v^{\mathrm{HF}} \tag{3}$$

and is nonpositive because of the variational principle.

DFT replaces the central role of the one-body potential with the ground-state density $n(\mathbf{r})$. From the Hohenberg−Kohn theorem,[27] there is (at most) one $v(\mathbf{r})$, which has a given density as its ground state, and from the variational principle, the ground state energy of system of $N$ electrons and external potential $v(\mathbf{r})$ is

$$E_v = \min_{n \to N} \left( F[n] + \int v(\mathbf{r}) n(\mathbf{r}) \mathrm{d}\mathbf{r} \right) \tag{4}$$

where $F[n]$ is the universal part of the Hohenberg−Kohn functional, defined as[28,29]

$$F[n] = \min_{\Psi \to n} \langle \Psi | \hat{T} + \hat{V}_{\mathrm{ee}} | \Psi \rangle \tag{5}$$

where $\hat{T}$ is the kinetic energy operator, $\hat{V}_{\mathrm{ee}}$ is the electron repulsion operator, and the minimization is over all antisymmetric wavefunctions that integrate to density $n(\mathbf{r})$. Denote the minimizer by $\Psi[n]$. The further ansatz of the KS scheme is that there exists a local multiplicative potential, $v_{\mathrm{S}}(\mathbf{r})$, whose ground-state density for noninteracting fermions matches the interacting one. The total energy in terms of KS quantities is then

$$E_v = \min_{n} \left( T_{\mathrm{S}}[n] + \int v(\mathbf{r}) n(\mathbf{r}) \mathrm{d}\mathbf{r} + E_{\mathrm{H}}[n] + E_{\mathrm{XC}}[n] \right) \tag{6}$$

where $T_{\mathrm{S}}$ is the kinetic energy of the KS electrons, $E_{\mathrm{H}}[n]$ is the Hartree energy, and $E_{\mathrm{XC}}[n]$ is the XC energy. The KS wavefunction is $\Phi_{\mathrm{S}}[n]$, which we take here to be a single Slater determinant, as is typical.

We highlight some subtle points that will be important in what follows. The quantum-mechanical operators are known, so each energy component has an obvious functional dependence on the wavefunction, such as

$$T[\Psi] = -\frac{1}{2} \sum_{i=1}^{N} \langle \Psi | \nabla_i^2 | \Psi \rangle \tag{7}$$

in atomic units. For any Slater determinant $\Phi = \{\chi\}_N$ of $N$ orbitals $\chi_i(\mathbf{x})$ of space-spin coordinate $\mathbf{x} = (\mathbf{r}, \sigma)$ and $\int \mathrm{d}\mathbf{x} = \sum_\sigma \int \mathrm{d}\mathbf{r}$

$$T[\Phi] = \frac{1}{2} \sum_{i=1}^{N} \int \mathrm{d}\mathbf{x} |\nabla \chi_i(\mathbf{x})|^2 \tag{8}$$

Density functionals are then defined *via* the minimizing wavefunctions. The KS kinetic energy is found by setting $\hat{V}_{\mathrm{ee}} = 0$ in eq 5

$$T_{\mathrm{S}}[n] = \min_{\Psi \to n} \langle \Psi | \hat{T} | \Psi \rangle = T\left[\Phi_{\mathrm{S}}[n]\right] \tag{9}$$

where $\Phi_{\mathrm{S}}[n]$ is the minimizer. The exact kinetic energy is

$$T[n] = T[\Psi[n]] \tag{10}$$

These two differ by the correlation kinetic energy

$$T_{\mathrm{C}}[n] = T[n] - T_{\mathrm{S}}[n] \tag{11}$$

which must be nonnegative, as $T_{\mathrm{S}}$ is the minimizer of $\hat{T}$ for the given density. Analogously, the exchange energy of $N$ orbitals is

$$E_{\mathrm{X}}[\Phi] = -\frac{1}{2} \sum_{i,j}^{N} \iint \mathrm{d}\mathbf{x}\, \mathrm{d}\mathbf{x}' \frac{\chi_i^*(\mathbf{x}) \chi_j^*(\mathbf{x}') \chi_j(\mathbf{x}) \chi_i(\mathbf{x}')}{\|\mathbf{r} - \mathbf{r}'\|} \tag{12}$$

which yields the exact exchange density functional in DFT

$$E_{\mathrm{X}}[n] = E_{\mathrm{X}}[\Phi_{\mathrm{S}}[n]] \tag{13}$$

The DFT definition of the correlation energy is then a density functional

$$\begin{aligned} E_{\mathrm{C}}[n] &= \langle \Psi[n] | \hat{H} | \Psi[n] \rangle - \langle \Phi_{\mathrm{S}}[n] | \hat{H} | \Phi_{\mathrm{S}}[n] \rangle \\ &= T_{\mathrm{C}}[n] + U_{\mathrm{C}}[n] \end{aligned} \tag{14}$$

where the potential contribution to correlation is

$$U_{\mathrm{C}}[n] = V_{\mathrm{ee}}[n] - E_{\mathrm{H}}[n] - E_{\mathrm{X}}[n] \tag{15}$$

For weakly correlated systems, such as atoms or most molecules, $T_{\mathrm{C}}$ has been found to be only slightly less than $|E_{\mathrm{C}}|$, so that $E_{\mathrm{C}} + T_{\mathrm{C}}$ which is nonpositive, is much smaller in magnitude than either. For example, for the He atom, $E_{\mathrm{C}}$ is −42 mH, $T_{\mathrm{C}}$ is 36 mH, and their sum is −6 mH,[30] and for the $Li_2$ molecule, $E_{\mathrm{C}}$ is −111 mH, $T_{\mathrm{C}}$ is 83 mH, and their sum is −28 mH.[31]

There are subtle differences between DFT and wavefunction theory.[32] As the HF Slater determinant minimizes $\hat{H}$ over all Slater determinants, whereas the KS Slater determinant is restricted to orbitals coming from a single multiplicative potential, the definition of correlation energy differs. For a given external potential

$$\Delta E_{\mathrm{C},v} = E_{\mathrm{C},v}^{\mathrm{trad}} - E_{\mathrm{C}}[n_v] \tag{16}$$

so that

$$\Delta E_{\mathrm{C},v} = \langle \Phi_{\mathrm{S}}[n_v] | \hat{H} | \Phi_{\mathrm{S}}[n_v] \rangle - \langle \Phi_v^{\mathrm{HF}} | \hat{H} | \Phi_v^{\mathrm{HF}} \rangle \tag{17}$$



https://dx.doi.org/10.1021/acs.jctc.0c00391
J. Chem. Theory Comput. 2020, 16, 5014−5023

must be nonnegative (although only very slightly, 0.1 mH for He).[32] A larger difference comes from the difference between the KS and HF Slater determinants, even when they refer to the same density. Define the density functional

$$\Delta T_S^{HF}[n] = T[\Phi_{v[n]}^{HF}] - T_S[n] \geq 0 \tag{18}$$

where $\Phi_{v[n]}^{HF}$ is the HF Slater determinant of $v[n](\mathbf{r})$, the one-body potential whose exact density is $n(\mathbf{r})$. We call $\Delta T_S^{HF}[n]$ the excess noninteracting HF kinetic energy. (In principle, this is found by adjusting $v(\mathbf{r})$ until an HF calculation yields $n(\mathbf{r})$ as its density.) This must be nonnegative, as the KS kinetic energy is the minimizer and can be several mH for mid-sized atoms.[33] Moreover, as $E[\Phi_{v[n]}^{HF}] \leq E[\Phi_S[n]]$, and both Hartree and one-body terms cancel,

$$\Delta E_X^{HF}[n] \leq -\Delta T_S^{HF}[n] \leq 0 \tag{19}$$

where we define the density functional

$$\Delta E_X^{HF}[n] = E_X[\Phi_{v[n]}^{HF}] - E_X[n] \tag{20}$$

We call $\Delta E_X^{HF}$ the excess HF exchange energy.

In the special case of atoms, the virial theorem guarantees that the total energy is exactly the negative of the kinetic energy for any minimized calculation, either exact, HF, or DFT with some XC functional. This implies that if $n$ is an exact atomic or atomic ion density

$$\Delta E_X^{HF} = -2\Delta T_S^{HF} \text{ (atoms or atomic ions)} \tag{21}$$

exactly. As the virial theorem only holds in the complete basis set limit, we never use it to calculate any energies but only to understand trends in the errors in the inversion process.

**2.2. KS Inversion.** The problem of finding accurate KS potentials for given densities has been studied almost as long as KS-DFT has been used.[15] There are now many algorithms in existence and use.[16,17,34−43] Some use just the density itself (a pure KS inversion), whereas others are focused on the most relevant case, that is, densities generated by a more accurate and controllable wavefunction calculation, in which case more information is available and can be used.[44−49] Here, we use two pure KS inversion schemes, Zhao−Morrison−Parr (ZMP)[37,50] and Wu−Yang (WY).[38] These methods may not be the best of all possible schemes but are suitable for our specific purpose, extracting the KS energy using only density. We always assume that the target density is pure-state noninteracting $v$-representable.

The solvers typically work by iteration. A guess for the desired KS potential is made, the KS orbitals are generated, the density is calculated, and the guessed potential is updated according to some algorithms. There are several relevant convergence criteria. The first is the choice of basis set for the inversion algorithm (note that this is independent of the basis set used to generate the target density). Second, there are often guiding functions for the guess. Because typical XC approximations have incorrect behavior of $v_S(\mathbf{r})$ far from nuclei, one often uses the Fermi−Amaldi (FA) potential,[51] which builds in the correct behavior. Third, in the case of the ZMP procedure, there is a penalty function for errors in the density, which is multiplied by a dimensionless parameter $\lambda$. As $\lambda \to \infty$, the procedure converges to the target density, but it can become unstable for too large values of $\lambda$.

Traditionally, such inversions are performed on accurate densities in order to gain insights into the exact KS quantities. The paradigmatic example is the extraordinary usefulness of the atomic KS potentials produced by Umrigar and co-workers.[19,20] Knowledge of the positions of the exact KS eigenvalues has been invaluable in tests of time-dependent DFT.[52,53]

However, the KS orbital energies are extremely sensitive to details of the potential, but ground-state energy differences (*e.g.*, reaction energies) are not. Below, we introduce just those quantities that are relevant to DC-DFT as criteria for sufficient convergence of the KS inversion. For a given inversion recipe, $n^{inv}(\mathbf{r})$ is a functional of the input or target density, $n(\mathbf{r})$, as are all the KS inversion orbitals and eigenvalues. For any energy functional of the density, we define the inversion error as

$$\Delta A^{inv}[n] = A[n^{inv}[n]] - A[n] \tag{22}$$

and we want this error to be sufficiently small so as not to obscure the reaction energies we wish to calculate.

The inversion error in a finite basis comes from several sources. First, a density from a multideterminantial wavefunction, that is, a correlated density, in a given finite atomic basis set typically cannot be exactly expressed as a KS density in that basis, and a more extensive basis set is required (see ref 54 for details). This problem only occurs when inverting a correlated target density. Although the basis set of the target density and inversion need not be the same in principle, we usually use the same basis set because ZMP and WY typically work with density matrices. Second, one cannot provide infinite flexibility to the KS potential in practice. In the case of ZMP, potential flexibility is limited to the size of the atomic orbital basis set. On the other hand, WY introduces a potential basis, which allows one to increase the flexibility of the potential by increasing the size of that basis. However, increased flexibility of the KS potential in WY may produce orbitals that are very close to the HF orbitals of the same density.[23] This makes the actual computation of eq 22 for the KS kinetic energy (*i.e.*, $A = T_S$) impossible because when $n^{inv}[n]$ approaches $n$, then simultaneously $T_S$ incorrectly approaches $T[\Phi_{v[n]}^{HF}]$. Nevertheless, in a subsequent section, we will show that this ambiguity is sufficiently small as to not invalidate our results.

**2.3. Density-Corrected DFT.** DC-DFT claims that, under well-understood conditions, the SC density in an approximate DFT calculation can contribute significantly to the error and that such error can usually be reduced by use of a more accurate density. The conventional measure for DFT error in energy is

$$\Delta E = \tilde{E}[\tilde{n}] - E[n] \tag{23}$$

where $E$ is the exact energy functional (of eq 6 in KS-DFT), and tilde denotes an approximation. One can define a functional error that comes from the approximate $\tilde{E}$ only, by

$$\Delta E_F = \tilde{E}[n] - E[n] = \tilde{E}_{XC}[n] - E_{XC}[n] \tag{24}$$

where the last equality holds in a KS calculation. The rest of the error comes from the $\tilde{n}(\mathbf{r})$ in the given energy functional

$$\Delta E_D = \Delta E - \Delta E_F = \tilde{E}[\tilde{n}] - \tilde{E}[n] \tag{25}$$

and is called the density-driven error.[2,11]

In DC-DFT, in principle, one should apply the approximate functional to the exact density for DFT calculations whose density-driven errors are significant (about 2 kcal/mol for small molecules[26]). By eliminating the density-driven error, the energy usually improves significantly.[10−14] In practice,



https://dx.doi.org/10.1021/acs.jctc.0c00391
J. Chem. Theory Comput. 2020, 16, 5014−5023

Table 1. Inversion Errors on a KS Density for Total Molecular Energy ($\Delta E$), Reaction Energy [$E_{rxn} = E(\text{mol}) - E(\text{atoms})$], and KS Kinetic Energy for Reactions, for PBE Calculations on NaCl, in aug-cc-pVTZ Basis[a]

| functional | | $\Delta E^{PBE}$ | | $\Delta E_{rxn}^{PBE}$ | | $\Delta T_{S,rxn}$ | |
|---|---|---|---|---|---|---|---|
| geometry | | $R_e$ | $R_s$ | $R_e$ | $R_s$ | $R_e$ | $R_s$ |
| guide | $\lambda$ | ZMP | | | | | |
| FA | 64 | 11.82 | 11.61 | 3.22 | 3.01 | −534 | −524 |
| | 128 | 7.08 | 6.90 | 1.62 | 1.44 | −309 | −300 |
| | 256 | 4.08 | 3.98 | 0.83 | 0.72 | −178 | −171 |
| | 512 | 2.06 | | 0.37 | | −101 | |
| SVWN | 64 | 0.40 | 0.39 | 0.01 | 0.00 | −4.88 | −3.96 |
| | 128 | 0.27 | 0.26 | 0.01 | 0.00 | −4.46 | −3.65 |
| | 256 | 0.17 | 0.16 | 0.01 | 0.00 | −3.68 | −2.70 |
| | 512 | 0.10 | | 0.01 | | −2.67 | |
| BLYP | 64 | 0.04 | 0.04 | 0.00 | 0.00 | −0.95 | −0.03 |
| | 128 | 0.02 | 0.02 | 0.00 | 0.00 | −1.28 | −0.22 |
| | 256 | 0.01 | 0.01 | 0.00 | 0.00 | −1.15 | −0.17 |
| | 512 | 0.01 | | 0.00 | | −0.83 | |
| guide | PBS | WY | | | | | |
| FA | D | 1.81 | 1.82 | −0.44 | −0.43 | 3.08 | 10.12 |
| | T | 0.53 | 0.34 | 0.06 | −0.13 | −3.01 | 0.40 |
| | CT | 0.03 | 0.02 | 0.01 | 0.00 | 0.28 | 0.25 |
| | CQ | 0.00 | 0.00 | 0.00 | 0.00 | 0.10 | 0.16 |
| SVWN | D | 0.34 | 0.49 | −0.03 | 0.11 | −3.60 | −0.48 |
| | T | 0.12 | 0.09 | 0.03 | 0.00 | −3.18 | −0.89 |
| | CT | 0.01 | 0.00 | 0.00 | 0.00 | 0.09 | 0.25 |
| | CQ | 0.00 | 0.00 | 0.00 | 0.00 | −0.03 | 0.21 |
| BLYP | D | 0.06 | 0.12 | −0.02 | 0.04 | −0.60 | 1.04 |
| | T | 0.02 | 0.02 | 0.00 | 0.00 | −1.31 | −0.25 |
| | CT | 0.00 | 0.00 | 0.00 | 0.00 | 0.36 | 0.26 |
| | CQ | 0.00 | 0.00 | 0.00 | 0.00 | 0.04 | 0.22 |

[a]Here, $R_e$ = 2.4 Å, $R_s$ = 4.5 Å, and blank cells denote that inversions are not converged. All energies are in miliHartree.

calculating highly accurate densities, such as from CCSD(T), is similar to or more expensive than simply running CCSD(T) to find energies. For molecular calculations, HF-DFT often suffices to yield significantly improved energetics when density-driven errors are large,[10−14,55−57] with little or no additional cost relative to the SC-DFT calculation. However, HF-DFT uses the HF orbitals, simply swapping the HF exchange for the approximate DFT XC, evaluated on the HF orbitals. This procedure ignores $\Delta T_S^{HF}$, the difference between HF and KS kinetic energies.

## 3. RESULTS AND DISCUSSION

Our aim is to test the WY and ZMP KS inversion schemes for use in validating the assumptions underlying HF-DFT. Thus, inversion errors in energies must be smaller than the density-driven errors that are (presumably) being eliminated by the HF-DFT procedure. In this section, we perform inversions targeting KS, HF, and correlated density and check the accuracy and precision of the inversion. As our prototypical choices, we consider the NaCl molecule, both at equilibrium ($R_e$ = 2.4 Å) and when stretched ($R_s$ = 4.5 Å). At equilibrium, most calculations with standard functionals are normal (DFT error has a negligible density-driven contribution), while most are abnormal when stretched.[2,11,12] Our default (standard) functional is PBE, and our default (standard) basis set is aug-cc-pVTZ. In addition to the commonly used FA guiding potential, approximate XC guiding potentials were also tested because our purpose is not to generate the shape of the exact KS potential but only to calculate the KS energy. We used two guiding potentials, SVWN and BLYP, as representative of semilocal functionals. Each guiding potential belongs to a different level of Jacob's ladder,[58] but the inversion results differ negligibly (discussed later). We introduce shorthand notations for the potential basis sets (PBS) for WY; X, CX, uCX, and ACX, stand for cc-pVXZ, cc-pCVXZ, unc-cc-pCVXZ, and aug-cc-pCVXZ, respectively, where X(=D, T, Q, 5) is the cardinal number of the PBS.

### 3.1. Approximate KS Target Density.

A simple consistency check is to take the density from a standard DFT calculation and run inversions to see how accurately we recover the KS energetic components, for which we have "exact" answers from the original calculation. To avoid trivial solutions, we used guiding potentials that are not used for the SC calculation. In the case of a KS target density, one can easily calculate eq 22 for the total energy because $T_S$ is known from the SC-KS calculation. Table 1 shows results for NaCl with PBE and its inverted densities. Several important lessons can be drawn from these results. First, errors in this inversion can be driven down to the microhartree range. Second, errors are typically reduced by tightening the convergence parameters, such as larger PBS, larger values of $\lambda$, or using guiding functionals that are close to the original functional that generated the density. Third, when convergence is an issue, total energy converges much faster than energy components, and reaction energies converge much faster than individual energies. Fourth, the FA guiding functional converges most slowly here, presumably because the PBE target density was generated from an XC functional yielding a different (and incorrect) asymptotic behavior. Nevertheless, for ZMP/FA, $\lambda$



https://dx.doi.org/10.1021/acs.jctc.0c00391
J. Chem. Theory Comput. 2020, 16, 5014−5023

= 512 yields sufficiently accurate reaction energies, (subscript rxn hereafter), so we chose to use $\lambda = 512$ as our default. In the case of WY, as the accuracy of $\Delta T_{S,rxn}$ is greatly improved when we increase PBS from T to CT, we chose CT, that is, cc-pCVTZ, as our default potential basis. In addition, for a given $\lambda$ and/or PBS condition, the difference between SVWN and BLYP is much smaller than the difference between BLYP and FA, so similar results are expected for any XC guiding potential at the LDA or GGA levels.

**3.2. HF Target Density.** Our first nontrivial task is to find $\Delta T_S^{HF}$, the contribution ignored in a typical HF-DFT calculation. An HF-DFT calculation first runs an HF calculation and then replaces the exchange term with the XC of KS-DFT. For any approximate XC functional, define

$$\tilde{V}_{exp}[n] = \int d\mathbf{r} n(\mathbf{r}) v(\mathbf{r}) + E_H[n] + \tilde{E}_{XC}[n] \tag{26}$$

the contributions to the energy that are known explicitly as functionals of the density. Then,

$$\tilde{E}^{HF\text{-}DFT} = T[\Phi_v^{HF}] + \tilde{V}_{exp}[n_v^{HF}] \tag{27}$$

However, DFT energies on HF densities are defined as

$$\tilde{E}[n^{HF}] = T_S[n^{HF}] + \tilde{V}_{exp}[n^{HF}] \tag{28}$$

Subtracting eq 28 from both sides of eq 27 when $n^{HF} = n_v^{HF}$ yields

$$\tilde{E}_v^{HF\text{-}DFT} - \tilde{E}[n_v^{HF}] = T[\Phi_v^{HF}] - T_S[n_v^{HF}] = \Delta T_s^{HF}[n_v^{HF}] \tag{29}$$

However, because of the uncertainty of the inversion, we cannot calculate $\tilde{E}[n^{HF}]$ or $T_S[n^{HF}]$ exactly. Instead, we calculate $\tilde{E}[n^{inv}[n^{HF}]]$ or $T_S[n^{inv}[n^{HF}]]$ *via* approximate inversion of the HF density. Because the total energy is much less sensitive to small changes of the density (here, inversion error) than individual energy components such as the kinetic energy, for the estimation of $\Delta T_S^{HF}$, we use

$$\Delta T_{S,est}^{HF} = \tilde{E}_v^{HF\text{-}DFT} - \tilde{E}[n^{inv}[n_v^{HF}]] \tag{30}$$

where the subscript est represents the estimated value.

Table 2 reports $\Delta T_{S,est}^{HF}$ values (eq 30) for Na and Cl atoms and reaction (atomization) energies of NaCl. Even with our standard protocol, the $\Delta T_S^{HF}$ of ZMP and WY in molecular energy varies by up to 2 mH. However, reaction energies are far less sensitive, and here variations are negligible. As the reaction energies of HF-PBE are −148 and −62 mH for equilibrium and stretched geometry, respectively, these variations are less than 1% of the reaction energy. Therefore, although obtaining a precise $\Delta T_S^{HF}$ is not possible with our methodology, estimations can be made precisely enough (within about ±0.5 mH) for reaction energies to be useful in testing HF-DFT.

**Table 2. Estimated $\Delta T_S^{HF}$ Values (Equation 30) for Equilibrium ($R_e$ = 2.4 Å) and Stretched ($R_s$ = 4.5 Å) Geometry of NaCl and for Corresponding Reaction Energies[a]**

| functional | | $\Delta T_{S,est}$ | | $\Delta T_{S,rxn,est}$ | |
|---|---|---|---|---|---|
| geometry | | $R_e$ | $R_s$ | $R_e$ | $R_s$ |
| guide | $\lambda$ | ZMP | | | |
| FA | 512 | 2.81 | 2.38 | 0.37 | −0.05 |
| BLYP | 512 | 2.36 | 1.95 | 0.22 | −0.18 |
| guide | PBS | WY | | | |
| FA | CT | 0.74 | 0.46 | −0.08 | −0.37 |
| | uC5 | 0.26 | 0.24 | 0.18 | 0.16 |
| BLYP | CT | 0.77 | 0.48 | −0.07 | −0.36 |

[a]All energies are in miliHartree.

In a WY inversion, $\Delta T_{S,est}^{HF}$ becomes very small when PBS is very large, for example, uC5. In the reaction energy calculation of NaCl, this does not cause a severe problem because $\Delta T_S^{HF}$ itself is very small. However, when $\Delta T_S^{HF}$ is large, then increasing the size of PBS will eventually cause $\Delta T_{S,est}^{HF}$ to vanish incorrectly. We find that a PBS with the same level of $\zeta$ plus tight core functions is balanced (giving an accurate density but not an unphysically small $\Delta T_{S,est}^{HF}$) with an atomic orbital basis. Also, $\Delta T_{S,est}^{HF}$ using different guiding potentials using CT PBS varies by less than 0.03 mH, indicating that CT is flexible enough to cover the differences in various guiding potentials. We thus report values of $\Delta T_S^{HF}$ for reaction energies only using WY and assuming uncertainties of ±0.5 mH.

To take advantage of error cancellations for $\Delta E_X^{HF}$, we define

$$\Delta E_{X,est}^{HF} = E_v^{HF} - \langle \Phi_S[n^{inv}[n_v^{HF}]] | \hat{H} | \Phi_S[n^{inv}[n_v^{HF}]] \rangle - \Delta T_{S,est}^{HF} \tag{31}$$

which are shown in Table 3. For each inversion, $\Delta E_{X,est}^{HF} < 0$ for total energies (eqs 18 and 19). Also, by comparing Tables 2 and 3, typically $\Delta E_{X,est}^{HF} \approx -2\Delta T_{S,est}^{HF}$, both for total and reaction energies, as expected from eq 21. Although eq 21 is satisfied exactly only for a complete basis with an exact inversion in the separated atom limit, we observed that the ratio $\Delta E_{X,rxn,est}^{HF}/\Delta T_{S,rxn,est}^{HF}$ is not dramatically far from −2 (see last two columns in Table 3) for WY. We expect this is because (1) neither $\Delta T_S^{HF}$ nor $\Delta T_X^{HF}$ was calculated directly from the definition but using eqs 30 and 31, which takes advantage of error cancelation and (2) although eq 21 is satisfied only in the separated atom limit, NaCl approximately satisfies it. In the case of ZMP on a stretched molecule, the ratio becomes meaningless, because the magnitudes of both $\Delta E_{X,est}^{HF}$ and $\Delta T_{S,est}^{HF}$ are too small to be accurate.

**Table 3. Estimated $\Delta E_X^{HF}$ Values for Equilibrium ($R_e$ = 2.4 Å) and Stretched ($R_s$ = 4.5 Å) Geometry of NaCl and for Corresponding Reaction Energies[a]**

| functional | | $\Delta E_{X,est}^{HF}$ | | $\Delta E_{X,rxn,est}^{HF}$ | | $\Delta E_X^{HF}/\Delta T_S^{HF}$ | |
|---|---|---|---|---|---|---|---|
| geometry | | $R_e$ | $R_s$ | $R_e$ | $R_s$ | $R_e$ | $R_s$ |
| guide | $\lambda$ | ZMP | | | | | |
| FA | 512 | −7.60 | −6.69 | −1.29 | −0.38 | −3.5 | 6.9 |
| BLYP | 512 | −3.70 | −2.94 | −0.70 | 0.06 | −3.1 | −0.4 |
| guide | PBS | WY | | | | | |
| FA | CT | −1.70 | −1.13 | 0.30 | 0.88 | −3.6 | −2.4 |
| | uC5 | −0.30 | −0.29 | −0.21 | −0.20 | −1.2 | −1.2 |
| BLYP | CT | −1.68 | −1.04 | 0.14 | 0.78 | −1.8 | −2.2 |

[a]All energies are in miliHartree. The last two columns show the ratio between $\Delta E_{X,rxn,est}^{HF}$ and $\Delta T_{S,rxn,est}^{HF}$.

**3.3. Correlated Target Density.** Now, we consider the inversion when targeting an electron density from a correlated coupled cluster singles, doubles (CCSD) wavefunction ($n^{CC}$). To check the quality of such an inversion, we extract $T_C$, the kinetic correlation energy, as accurately as practical. Just as for



https://dx.doi.org/10.1021/acs.jctc.0c00391
J. Chem. Theory Comput. 2020, 16, 5014−5023

HF, to take advantage of error cancellations, we define, analogous to eq 27

$$\tilde{E}_v^{\text{TC-DFT}} = T[\Psi_v^{\text{CC}}] + \tilde{V}_{\text{exp}}[n_v^{\text{CC}}] \tag{32}$$

where $T$ is the value from the CCSD calculation. We can then estimate $T_C$ analogously to eq 30

$$T_{C,\text{est}} = \tilde{E}_v^{\text{TC-DFT}} - \tilde{E}[n^{\text{inv}}[n_v^{\text{CC}}]] \tag{33}$$

Similar to Table 2, standard ZMP and WY give different estimates of $T_C$ (by approximately 1.2 mH), but this variation is much smaller in reaction energies (approximately 0.1 mH). (As CCSD is not variational, the virial relation cannot be used.)

From Tables 2 and 4, it seems not possible to obtain exact $\Delta T_S^{\text{HF}}$ or $T_C$ values because of the fundamental limitations of the inversion methods. However, the two different inversion algorithms, ZMP and WY, yield consistent estimates for $\Delta T_{S,\text{rxn}}^{\text{HF}}$ and $T_{C,\text{rxn}}$. Therefore, we expect that inversion can provide $\tilde{E}[n]$ with a minor uncertainty, allowing density-driven error estimates with a useful level of accuracy. As the deviation of $\Delta T_{S,\text{rxn,est}}^{\text{HF}}$ in Table 2 was up to 0.5 mH, we expect that the exact inversion results to be within ±0.5 kcal/mol when calculated under standard inversion conditions. (Note that 1 mH < 1 kcal/mol.) In the next subsection, as a practical application of the inversion, we will present the entire dissociation curves of NaCl and $OH{\cdot}Cl^-$.

**Table 4. Estimated $T_C$ Values for Equilibrium ($R_e$ = 2.4 Å) and Stretched ($R_s$ = 4.5 Å) NaCl and for Corresponding Reaction Energies**[a]

| functional | | $T_{C,\text{est}}$ | | $T_{C,\text{rxn,est}}$ | |
|---|---|---|---|---|---|
| geometry | | $R_e$ | $R_s$ | $R_e$ | $R_s$ |
| guide | $\lambda$ | ZMP | | | |
| FA | 512 | 193.10 | 189.01 | 21.77 | 17.68 |
| BLYP | 512 | 193.12 | 189.07 | 21.80 | 17.74 |
| guide | PBS | WY | | | |
| FA | CT | 191.94 | 187.77 | 21.85 | 17.68 |
| BLYP | CT | 191.97 | 187.78 | 21.87 | 17.68 |

[a]Estimations were made using eq 33. All energies are in miliHartree.

**3.4. Testing HF-DFT.** Previously, it was argued that the poor description of SC-DFT calculations for dissociation limits of heterodiatomic molecules was due to density-driven error and HF-DFT reduces that error.[2,12] Here, we test the argument by quantitatively decomposing the DFT (here, PBE) error using a highly accurate CCSD density as a benchmark. (CCSD(T) density shows no meaningful differences, see Table S10 in the Supporting Information.) In these calculations, all inversions were performed using the WY algorithm, FA guiding potential, and CT potential basis (WY/FA/CT). Figure 1 presents dissociation curves of the NaCl molecule.

Whereas SC-PBE does not account for the correct dissociation behavior, making a huge well-known error in the dissociation limit,[59] DC-PBE with the inversion of the HF or CCSD densities (DC-PBE[HF] and DC-PBE[CC], respectively) correctly captures the dissociation limit, although they are slightly above CCSD(T). Note that the HF-PBE curve is obtained from eq 27, while the DC-PBE[HF] curve is obtained from eq 28 with inverted HF density. Most importantly, HF-DFT and either of these curves are indistinguishable, showing

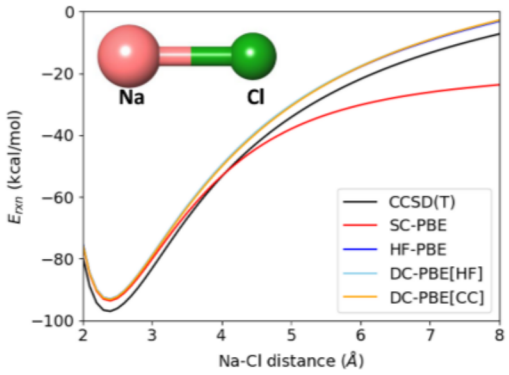


**Figure 1.** Dissociation curve of the NaCl molecule using CCSD(T), SC-PBE, HF-PBE, and DC-PBE using HF or CCSD density, using WY/FA/CT inversion. HF-PBE is calculated by eq 27, whereas DC-PBE[HF] is calculated by eq 28. HF-PBE and DC-PBE[HF and CC] are indistinguishable on this scale. The criterion for the inversion imprecision, ±0.5 kcal/mol, is similar to the scale of the thickness of the lines.

that HF-DFT differs negligibly from PBE energies evaluated on (essentially) exact densities. This validates the use of HF-DFT as a practical approximation to DC-DFT. Although we have defined density-driven error only for SC-DFT calculations, the density-driven error can be defined for any approximate XC energy for non-SC-DFT by replacing $\tilde{n}$ in eq 25 by any non-SC density.[8] By doing so, we can calculate the density-driven error of $n^{\text{HF}}$.

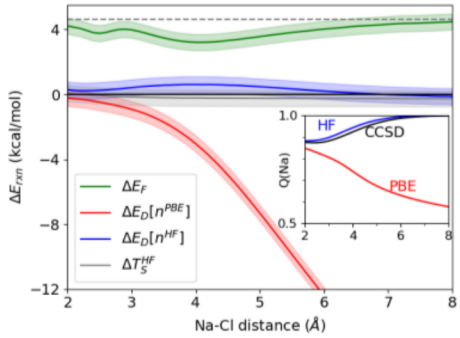


**Figure 2.** Functional error $\Delta E_F$ and density-driven error $\Delta E_D$ of $n^{\text{PBE}}$ and $n^{\text{HF}}$ and $\Delta T_S^{\text{HF}}$ of NaCl dissociation curve. Curves are drawn with ±0.5 kcal/mol bands to represent the uncertainty of the inversion. $\Delta T_S^{\text{HF}}$ is almost indistinguishable from zero. The gray dashed horizontal line (4.6 kcal/mol) represents $\Delta E_F$ of the reaction Na + Cl → $Na^+$ + $Cl^-$. The inset shows the intrinsic atomic orbitals (IAO) population of the Na atom.

To further study the differences between these curves, Figure 2 shows the small differences between the curves in Figure 1. We write

$$\Delta E_{F,v} = \Delta E_v^{\text{HF-DFT}} - \Delta E_D[n_v^{\text{HF}}] - \Delta T_S^{\text{HF}}[n_v^{\text{HF}}] \tag{34}$$

by combining eqs 24, 25, and 29, where $\Delta E_D[n^{\text{HF}}] = \tilde{E}[n^{\text{HF}}] - \tilde{E}[n]$ is the PBE density-driven error of the HF density. Curves are drawn with ±0.5 kcal/mol bands to represent the uncertainty of the inversion. $\Delta E_F$ in Figure 2 is almost constant regardless of the geometry. Thus, on the scale of the



https://dx.doi.org/10.1021/acs.jctc.0c00391
J. Chem. Theory Comput. 2020, 16, 5014−5023

PBE density-driven errors, our imperfect inversions definitely show that the functional error estimated by HF-DFT barely differs from the true value.

On the other hand, $\Delta E_D[n^{PBE}]$ grows strongly with Na−Cl distance, directly showing the density delocalization error of PBE. We observed almost zero $\Delta E_D[n^{HF}]$ for any geometry in Figure 2. The behavior of $\Delta E_D$ can also be understood from population analysis. Here, we used Mulliken population analysis using IAO[60] constructed from KS orbitals of either PBE or an inversion (HF or CCSD). Note that IAO cannot be constructed directly from a correlated wavefunction, which requires KS inversion. The results are shown in the inset of Figure 2. At an Na−Cl distance of 2 Å, the population difference between CCSD and PBE is 0.03, which has almost no effect on $\Delta E_D[n^{PBE}]$. The population difference between HF and CCSD is maximum when the Na−Cl distance is near 4 Å. This difference is reflected in the error curve, where $\Delta E_D[n^{HF}]$ becomes slightly positive at that geometry. $\Delta T_S^{HF}$ is negligibly small everywhere (−0.08 and −0.37 mH for Na−Cl distance 2.4 and 4.5 Å, respectively, see Table 2). The population of the Na atom drops to zero after 8 Å, where the triplet state becomes the ground state (not shown).[12]

Finally, we point out that the functional error in the reaction $Na + Cl \rightarrow Na^+ + Cl^-$ (marked by the dashed horizontal line in Figure 2) dominates the $\Delta E_F$ in Figure 2. Thus, when measured relative to this limit, the error in a PBE curve evaluated on CC densities is < 2 kcal/mol everywhere!

As another example from a previous successful application of HF-DFT,[12] we also analyzed the potential energy curve of the linear $HO{\cdot}Cl^-$ complex (O−H distance fixed to 1 Å) in Figure 3. Here, we used augmented PBS (ACT) for WY because of

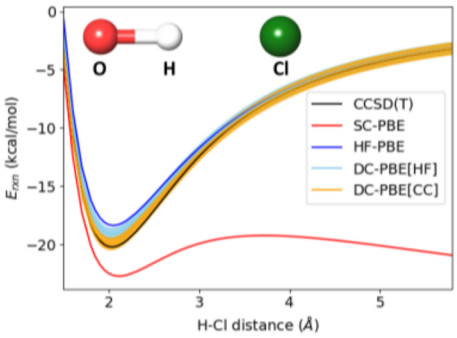


**Figure 3.** Dissociation curve of $OH{\cdot}Cl^-$ complex using CCSD(T), SC-PBE, HF-PBE, and DC-PBE with HF and CCSD density, using inversion. HF-PBE is calculated by eq 27, while DC-PBE[HF] is calculated by eq 28. DC-PBE curves are drawn with ±0.5 kcal/mol bands to represent the uncertainty of the inversion. All inversions were performed with WY/FA/ACT.

the WY convergence issue for H−Cl beyond 4 Å. SC-PBE shows a significant deviation from CCSD(T), not only in the stretched geometry but even in the equilibrium geometry. The DC-PBE[CC] curve almost coincides with the reference CCSD(T), showing that $\Delta E_F$ of the PBE functional is almost zero. On the other hand, DC-PBE[HF] and HF-PBE lie slightly higher than CCSD(T) and differ from each other. HF-PBE, DC-PBE[HF], and DC-PBE[CC] become closer to CCSD(T) as the H−Cl distance increases. Therefore, once again, HF-PBE greatly improves over SC-PBE, but more accurate densities with inversions yield slightly better results.

It is noticeable that the partial charges of the Cl fragment for any geometries are similar to the charge at the dissociation limit, as in the inset of Figure 4. (Note that this reflects charge

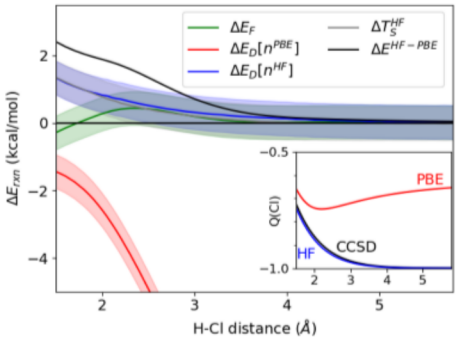


**Figure 4.** Error components of PBE and $\Delta T_S^{HF}$ of the $OH{\cdot}Cl^-$ dissociation curve. To represent the uncertainty of the inversion, curves are drawn as ±0.5 kcal/mol bands. $\Delta E_D[n^{HF}]$ and $\Delta T_S^{HF}$ are almost overlapped with each other. The inset shows the IAO population of the Cl atom. The error of HF-PBE is shown in a black solid line with no band because there is no inaccuracy because of inversion.

transfer from $Cl^-$ to OH. See Figure S1 in the Supporting Information for the partial charges of other atoms). The behaviors of $\Delta E_D[n^{PBE}]$ and $\Delta E_D[n^{HF}]$ are similar to that of NaCl. However, $\Delta T_S^{HF}$ is not negligibly small for short H−Cl distances; it almost overlaps with $\Delta E_D[n^{HF}]$ in Figure 4. $\Delta T_S^{HF}$ need not be zero for any reaction. The success of HF-PBE requires only that it be much smaller than $|\Delta E_D|$ whenever $|\Delta E_D(PBE)| > 2$ kcal/mol.

Of course, in most DFT calculations, the error of SC-DFT does not originate from large $\Delta E_D$. For some systems (such as spin-contaminated or strongly correlated[31]), the HF density is not a good approximation to the accurate density. The examples shown here have small $\Delta E_F$, small $\Delta E_D[n^{HF}]$, and large $\Delta E_D[n^{PBE}]$ and so are greatly improved by the use of HF-DFT.

## 4. CONCLUSIONS

We have shown here the reliability of the present KS inversion methods for the calculation of the density-driven and functional errors of common KS-DFT. Some known issues prohibit exact KS inversions in localized basis sets. From KS inversion methods, ZMP and WY, we show that these issues have a minor effect on reaction energies (sub-kcal/mol), when the inversion is performed with proper conditions; such as an approximate guiding potential, $\lambda$ in ZMP, or potential basis set in WY. Our recommendations are as follows:

(1) In the case of ZMP, a KS-DFT guiding potential works better than FA, even for the inversion of a non-KS density. On the other hand, results are not sensitive to the guiding potential in WY.
(2) Large $\lambda$ for ZMP: practically 512 suffices; a larger $\lambda$ may lead to convergence issues.
(3) For the potential basis set in WY, using a basis with the same level of $\zeta$ as the atomic orbital basis in addition to tight-core functions.

Under these conditions, one can accurately estimate the density-driven and functional error of common KS-DFT


https://dx.doi.org/10.1021/acs.jctc.0c00391
J. Chem. Theory Comput. 2020, 16, 5014−5023

calculations and also estimate the small errors introduced by the HF-DFT procedure. We expect that calculation of these errors will help the development of new XC functionals that reduce both $\Delta E_D$ and $\Delta E_F$.

## 5. COMPUTATIONAL DETAILS

CCSD is used as a reference density, while perturbative triples (CCSD(T)) is used as a reference of energy. All HF, DFT, and CC calculations were performed using a PySCF program package.[61] As we used PBE[62] as the default energy functional, FA, SVWN,[63,64] and BLYP[65,66] are tested as guiding potentials for inversions. The unrestricted scheme is used for open-shell systems. No frozen-core approximations were made for CC calculations. The aug-cc-pVTZ atomic orbital basis set is used for both the NaCl molecule and the $HO{\cdot}Cl^-$ complex.[67−69] We set the gradient converge threshold (conv_tol_grad attribute in the SCF base class in PySCF) for HF to $1 \times 10^{-7}$ to generate accurate reference HF determinant for CC calculations. For the convergence of PBE on the stretched molecules, we set level_shift = 0.2 and conv_check = False. All ZMP and WY calculations were conducted with our codes. For ZMP, we used direct inversion of iterative subspace algorithm[70] to accelerate convergence. We solved ZMP equations self-consistently for a $\lambda$ and used the output density matrix as an initial guess of the next ZMP equation with a larger $\lambda$. We say ZMP fails to converge at $\lambda'$ when it fails to converge when the initial guess density matrix is from $\lambda' - 1$. For WY, we used the Broyden−Fletcher−Goldfarb−Shanno algorithm[71] implemented in SciPy[72] for the optimization of the KS potential.

## ■ ASSOCIATED CONTENT

### Supporting Information

The Supporting Information is available free of charge at https://pubs.acs.org/doi/10.1021/acs.jctc.0c00391.

Inversion results of CCSD and CCSD(T) densities for NaCl and ZMP results for the $HO{\cdot}Cl^-$ complex (PDF)

## ■ AUTHOR INFORMATION


### Corresponding Author

**Eunji Sim** − *Department of Chemistry, Yonsei University, Seoul 03722, Korea;* orcid.org/0000-0002-4139-0960; Email: esim@yonsei.ac.kr

### Authors

**Seungsoo Nam** − *Department of Chemistry, Yonsei University, Seoul 03722, Korea;* orcid.org/0000-0001-9948-6140

**Suhwan Song** − *Department of Chemistry, Yonsei University, Seoul 03722, Korea;* orcid.org/0000-0002-7768-6181

**Kieron Burke** − *Departments of Chemistry and of Physics, University of California, Irvine, California 92697, United States*

Complete contact information is available at: https://pubs.acs.org/10.1021/acs.jctc.0c00391


### Notes

The authors declare no competing financial interest.

## ■ ACKNOWLEDGMENTS

This work at Yonsei University was supported by the grant from the Korean Research Foundation (2020R1A2C2007468). K.B. acknowledges NSF for Grant CHE 1856165.

## ■ REFERENCES


(1) Kohn, W.; Sham, L. J. Self-consistent equations including exchange and correlation effects. *Phys. Rev.* **1965**, *140*, A1133.

(2) Kim, M.-C.; Sim, E.; Burke, K. Understanding and reducing errors in density functional calculations. *Phys. Rev. Lett.* **2013**, *111*, 073003.

(3) Cohen, A. J.; Mori-Sanchez, P.; Yang, W. Insights into current limitations of density functional theory. *Science* **2008**, *321*, 792−794.

(4) Johnson, E. R.; Otero-De-La-Roza, A.; Dale, S. G. Extreme density-driven delocalization error for a model solvated-electron system. *J. Chem. Phys.* **2013**, *139*, 184116.

(5) Sosa Vazquez, X. A.; Isborn, C. M. Size-dependent error of the density functional theory ionization potential in vacuum and solution. *J. Chem. Phys.* **2015**, *143*, 244105.

(6) LeBlanc, L. M.; Dale, S. G.; Taylor, C. R.; Becke, A. D.; Day, G. M.; Johnson, E. R. Pervasive Delocalisation Error Causes Spurious Proton Transfer in Organic Acid−Base Co-Crystals. *Angew. Chem.* **2018**, *130*, 15122−15126.

(7) Wasserman, A.; Nafziger, J.; Jiang, K.; Kim, M.-C.; Sim, E.; Burke, K. The importance of being inconsistent. *Annu. Rev. Phys. Chem.* **2017**, *68*, 555−581.

(8) Vuckovic, S.; Song, S.; Kozlowski, J.; Sim, E.; Burke, K. Density functional analysis: The theory of density-corrected DFT. *J. Chem. Theory Comput.* **2019**, *15*, 6636−6646.

(9) http://tccl.yonsei.ac.kr/mediawiki/index.php/DC-DFT (accessed Apr 20, 2020).

(10) Kim, M.-C.; Sim, E.; Burke, K. Communication: Avoiding unbound anions in density functional calculations. *J. Chem. Phys.* **2011**, *134*, 171103.

(11) Kim, M.-C.; Sim, E.; Burke, K. Ions in solution: Density corrected density functional theory (DC-DFT). *J. Chem. Phys.* **2014**, *140*, 18A528.

(12) Kim, M.-C.; Park, H.; Son, S.; Sim, E.; Burke, K. Improved DFT potential energy surfaces via improved densities. *J. Phys. Chem. Lett.* **2015**, *6*, 3802−3807.

(13) Song, S.; Kim, M.-C.; Sim, E.; Benali, A.; Heinonen, O.; Burke, K. Benchmarks and reliable DFT results for spin gaps of small ligand Fe (II) complexes. *J. Chem. Theory Comput.* **2018**, *14*, 2304−2311.

(14) Kim, Y.; Song, S.; Sim, E.; Burke, K. Halogen and Chalcogen Binding Dominated by Density-Driven Errors. *J. Phys. Chem. Lett.* **2018**, *10*, 295−301.

(15) Almbladh, C. O.; Pedroza, A. C. Density-functional exchange-correlation potentials and orbital eigenvalues for light atoms. *Phys. Rev. A: At., Mol., Opt. Phys* **1984**, *29*, 2322.

(16) Aryasetiawan, F.; Stott, M. J. Effective potentials in density-functional theory. *Phys. Rev. B: Condens. Matter Mater. Phys.* **1988**, *38*, 2974.

(17) Van Leeuwen, R.; Baerends, E. J. Exchange-correlation potential with correct asymptotic behavior. *Phys. Rev. A: At., Mol., Opt. Phys* **1994**, *49*, 2421.

(18) Gritsenko, O. V.; Baerends, E. J. Effect of molecular dissociation on the exchange-correlation Kohn-Sham potential. *Phys. Rev. A: At., Mol., Opt. Phys* **1996**, *54*, 1957.

(19) Umrigar, C. J.; Gonze, X. Accurate exchange-correlation potentials and total-energy components for the helium isoelectronic series. *Phys. Rev. A: At., Mol., Opt. Phys* **1994**, *50*, 3827.

(20) Browne, D. A.; Callaway, J.; Draayer, J. P.; Haymaker, R. W.; Kalia, R. K.; Tohline, J. E.; Vashishta, P. Comparison of approximate and exact density functionals: A quantum monte carlo study, Umrigar, Cyrus J and Gonze, Xavier. *High Performance Computing and its Applications in the Physical Sciences: Proceedings of the Mardi Gras' 93 Conference*, 1994; pp 1−274.

(21) Bartlett, R. J.; Grabowski, I.; Hirata, S.; Ivanov, S. The exchange-correlation potential in ab initio density functional theory. *J. Chem. Phys.* **2005**, *122*, 034104.

(22) Hirata, S.; Ivanov, S.; Grabowski, I.; Bartlett, R. J.; Burke, K.; Talman, J. D. Can optimized effective potentials be determined uniquely? *J. Chem. Phys.* **2001**, *115*, 1635−1649.

(23) Staroverov, V. N.; Scuseria, G. E.; Davidson, E. R. Optimized effective potentials yielding Hartree-Fock energies and densities. *J. Chem. Phys.* **2006**, *124*, 141103.
(24) Heaton-Burgess, T.; Bulat, F. A.; Yang, W. Optimized effective potentials in finite basis sets. *Phys. Rev. Lett.* **2007**, *98*, 256401.
(25) Kollmar, C.; Neese, F. The static response function in Kohn-Sham theory: An appropriate basis for its matrix representation in case of finite AO basis sets. *J. Chem. Phys.* **2014**, *141*, 134106.
(26) Sim, E.; Song, S.; Burke, K. Quantifying Density Errors in DFT. *J. Phys. Chem. Lett.* **2018**, *9*, 6385−6392.
(27) Hohenberg, P.; Kohn, W. Inhomogeneous electron gas. *Phys. Rev.* **1964**, *136*, B864.
(28) Levy, M. Universal variational functionals of electron densities, first-order density matrices, and natural spin-orbitals and solution of the v-representability problem. *Proc. Natl. Acad. Sci. U.S.A.* **1979**, *76*, 6062−6065.
(29) Lieb, E. H. Density Functionals for CouIomb Systems. *Int. J. Quantum Chem.* **1983**, *24*, 243−277.
(30) Huang, C.-J.; Umrigar, C. J. Local correlation energies of two-electron atoms and model systems. *Phys. Rev. A: At., Mol., Opt. Phys* **1997**, *56*, 290.
(31) Gritsenko, O. V.; Schipper, P. R. T.; Baerends, E. J. Exchange and correlation energy in density functional theory: comparison of accurate density functional theory quantities with traditional Hartree−Fock based ones and generalized gradient approximations for the molecules Li2, N2, F2. *J. Chem. Phys.* **1997**, *107*, 5007−5015.
(32) Gross, E. K. U.; Petersilka, M.; Grabo, T. Conventional quantum chemical correlation energy versus density-functional correlation energy. *Chemical Applications of Density-Functional Theory*; ACS Symposium Series; ACS, 1996; Vol. *629*, pp 42−53.
(33) Görling, A.; Ernzerhof, M. Energy differences between Kohn-Sham and Hartree-Fock wave functions yielding the same electron density. *Phys. Rev. A: At., Mol., Opt. Phys* **1995**, *51*, 4501.
(34) Nagy, A.; March, N. H. One-body potential theory in terms of the phase of wave functions for the ground state of the Be atom. *Phys. Rev. A: At., Mol., Opt. Phys* **1989**, *39*, 5512.
(35) Görling, A. Kohn-Sham potentials and wave functions from electron densities. *Phys. Rev. A: At., Mol., Opt. Phys* **1992**, *46*, 3753.
(36) Wang, Y.; Parr, R. G. Construction of exact Kohn-Sham orbitals from a given electron density. *Phys. Rev. A: At., Mol., Opt. Phys* **1993**, *47*, R1591.
(37) Zhao, Q.; Morrison, R. C.; Parr, R. G. From electron densities to Kohn-Sham kinetic energies, orbital energies, exchange-correlation potentials, and exchange-correlation energies. *Phys. Rev. A: At., Mol., Opt. Phys* **1994**, *50*, 2138.
(38) Wu, Q.; Yang, W. A direct optimization method for calculating density functionals and exchange−correlation potentials from electron densities. *J. Chem. Phys.* **2003**, *118*, 2498−2509.
(39) Ryabinkin, I. G.; Staroverov, V. N. Determination of Kohn−Sham effective potentials from electron densities using the differential virial theorem. *J. Chem. Phys.* **2012**, *137*, 164113.
(40) Zhang, X.; Carter, E. A. Kohn-Sham potentials from electron densities using a matrix representation within finite atomic orbital basis sets. *J. Chem. Phys.* **2018**, *148*, 034105.
(41) Jensen, D. S.; Wasserman, A. Numerical methods for the inverse problem of density functional theory. *Int. J. Quantum Chem.* **2018**, *118*, No. e25425.
(42) Finzel, K.; Ayers, P. W.; Bultinck, P. A simple algorithm for the Kohn−Sham inversion problem applicable to general target densities. *Theor. Chem. Acc.* **2018**, *137*, 30.
(43) Kanungo, B.; Zimmerman, P. M.; Gavini, V. Exact exchange-correlation potentials from ground-state electron densities. *Nat. Commun.* **2019**, *10*, 4497.
(44) Ryabinkin, I. G.; Kananenka, A. A.; Staroverov, V. N. Accurate and efficient approximation to the optimized effective potential for exchange. *Phys. Rev. Lett.* **2013**, *111*, 013001.
(45) Cuevas-Saavedra, R.; Ayers, P. W.; Staroverov, V. N. Kohn−Sham exchange-correlation potentials from second-order reduced density matrices. *J. Chem. Phys.* **2015**, *143*, 244116.
(46) Ryabinkin, I. G.; Kohut, S. V.; Staroverov, V. N. Reduction of electronic wave functions to Kohn-Sham effective potentials. *Phys. Rev. Lett.* **2015**, *115*, 083001.
(47) Cuevas-Saavedra, R.; Staroverov, V. N. Exact expressions for the Kohn−Sham exchange-correlation potential in terms of wave-function-based quantities. *Mol. Phys.* **2016**, *114*, 1050−1058.
(48) Ospadov, E.; Ryabinkin, I. G.; Staroverov, V. N. Improved method for generating exchange-correlation potentials from electronic wave functions. *J. Chem. Phys.* **2017**, *146*, 084103.
(49) Ospadov, E.; Staroverov, V. N. Construction of Fermi Potentials from Electronic Wave Functions. *J. Chem. Theory Comput.* **2018**, *14*, 4246−4253.
(50) Zhao, Q.; Parr, R. G. Quantities T s [n] and T c [n] in density-functional theory. *Phys. Rev. A: At., Mol., Opt. Phys.* **1992**, *46*, 2337.
(51) Fermi, E.; Amaldi, E. Le orbite infinito degli elementi. *Accad. Ital.* **1934**, *6*, 117.
(52) Savin, A.; Umrigar, C. J.; Gonze, X. Relationship of Kohn−Sham eigenvalues to excitation energies. *Chem. Phys. Lett.* **1998**, *288*, 391−395.
(53) Van Meer, R.; Gritsenko, O. V.; Baerends, E. J. Physical meaning of virtual Kohn−Sham orbitals and orbital energies: an ideal basis for the description of molecular excitations. *J. Chem. Theory Comput.* **2014**, *10*, 4432−4441.
(54) Mayer, I.; Pápai, I.; Bakó, I.; Nagy, Á. Conceptual problem with calculating electron densities in finite basis density functional theory. *J. Chem. Theory Comput.* **2017**, *13*, 3961−3963.
(55) Gill, P. M. W.; Johnson, B. G.; Pople, J. A.; Frisch, M. J. An investigation of the performance of a hybrid of Hartree-Fock and density functional theory. *Int. J. Quantum Chem.* **1992**, *44*, 319−331.
(56) Janesko, B. G.; Scuseria, G. E. Hartree−Fock orbitals significantly improve the reaction barrier heights predicted by semilocal density functionals. *J. Chem. Phys.* **2008**, *128*, 244112.
(57) Verma, P.; Perera, A.; Bartlett, R. J. Increasing the applicability of DFT I: Non-variational correlation corrections from Hartree−Fock DFT for predicting transition states. *Chem. Phys. Lett.* **2012**, *524*, 10−15.
(58) Perdew, J. P.; Schmidt, K. Jacob's ladder of density functional approximations for the exchange-correlation energy. *AIP Conference Proceedings*; AIP, 2001; pp 1−20.
(59) Ruzsinszky, A.; Perdew, J. P.; Csonka, G. I.; Vydrov, O. A.; Scuseria, G. E. Spurious fractional charge on dissociated atoms: Pervasive and resilient self-interaction error of common density functionals. *J. Chem. Phys.* **2006**, *125*, 194112.
(60) Knizia, G. Intrinsic atomic orbitals: An unbiased bridge between quantum theory and chemical concepts. *J. Chem. Theory Comput.* **2013**, *9*, 4834−4843.
(61) Sun, Q.; Berkelbach, T. C.; Blunt, N. S.; Booth, G. H.; Guo, S.; Li, Z.; Liu, J.; McClain, J. D.; Sayfutyarova, E. R.; Sharma, S.; Wouters, S.; Chan, G. K. L. PySCF: the Python-based simulations of chemistry framework. *Wiley Interdiscip. Rev.: Comput. Mol. Sci.* **2018**, *8*, No. e1340.
(62) Perdew, J. P.; Burke, K.; Ernzerhof, M. Generalized gradient approximation made simple. *Phys. Rev. Lett.* **1996**, *77*, 3865.
(63) Dirac, P. A. M. Note on exchange phenomena in the Thomas atom. *Math. Proc. Camb. Phil. Soc.* **1930**, *26*, 376−385.
(64) Vosko, S. H.; Wilk, L.; Nusair, M. Accurate spin-dependent electron liquid correlation energies for local spin density calculations: a critical analysis. *Can. J. Phys.* **1980**, *58*, 1200−1211.
(65) Becke, A. D. Density-functional exchange-energy approximation with correct asymptotic behavior. *Phys. Rev. A: At., Mol., Opt. Phys* **1988**, *38*, 3098.
(66) Lee, C.; Yang, W.; Parr, R. G. Development of the Colle-Salvetti correlation-energy formula into a functional of the electron density. *Phys. Rev. B: Condens. Matter Mater. Phys.* **1988**, *37*, 785.
(67) Dunning, T. H. Gaussian basis sets for use in correlated molecular calculations. I. The atoms boron through neon and hydrogen. *J. Chem. Phys.* **1989**, *90*, 1007−1023.


https://dx.doi.org/10.1021/acs.jctc.0c00391
*J. Chem. Theory Comput.* 2020, 16, 5014−5023

(68) Kendall, R. A.; Dunning, T. H., Jr.; Harrison, R. J. Electron affinities of the first-row atoms revisited. Systematic basis sets and wave functions. *J. Chem. Phys.* **1992**, *96*, 6796−6806.
(69) Woon, D. E.; Dunning, T. H., Jr. Gaussian basis sets for use in correlated molecular calculations. III. The atoms aluminum through argon. *J. Chem. Phys.* **1993**, *98*, 1358−1371.
(70) Pulay, P. Convergence acceleration of iterative sequences. The case of SCF iteration. *Chem. Phys. Lett.* **1980**, *73*, 393−398.
(71) Nocedal, J.; Wright, S. *Numerical Optimization*; Springer Science & Business Media, 2006.
(72) Virtanen, P.; Gommers, R.; Oliphant, T. E.; Haberland, M.; Reddy, T.; Cournapeau, D.; Burovski, E.; Peterson, P.; Weckesser, W.; Bright, J.; van der Walt, S. J.; Brett, M.; Wilson, J.; Millman, K. J.; Mayorov, N.; Nelson, A. R. J.; Jones, E.; Kern, R.; Larson, E.; Carey, C. J.; Polat, İ.; Feng, Y.; Moore, E. W.; VanderPlas, J.; Laxalde, D.; Perktold, J.; Cimrman, R.; Henriksen, I.; Quintero, E. A.; Harris, C. R.; Archibald, A. M.; Ribeiro, A. H.; Pedregosa, F.; van Mulbregt, P. SciPy 1.0: Fundamental Algorithms for Scientific Computing in Python. *Nat. Methods* **2020**, *17*, 261−272.



https://dx.doi.org/10.1021/acs.jctc.0c00391
*J. Chem. Theory Comput.* 2020, 16, 5014−5023